Accessing diverse azole carboxylic acid building blocks via mild C-H carboxylation: Parallel, one-pot amide couplings and ML-guided substrate scope design

S. Felten[‡*], C. Q. He[§*], M. Weisel[‡], M. Shevlin[‡] and M. H. Emmert[‡*]

[‡]Process Research & Development, MRL, Merck & Co. Inc, 126 E Lincoln Ave, Rahway, NJ 07065, USA.

[§]Computational and Structural Chemistry, MRL, Merck & Co. Inc, 126 E Lincoln Ave, Rahway, NJ 07065, USA.

Supporting Information Placeholder

ABSTRACT: This manuscript describes a mild, functional group tolerant, and metal-free C-H carboxylation that enables direct access to azole-2-carboxylic acids, followed by amide couplings in one pot. This sequence accesses a large variety of azole-2-amides, demonstrating the significant expansion of the accessible chemical space, as compared to previously known methodologies. Key to the described reactivity is the use of silyl triflate reagents, which serve as reaction mediators in C-H deprotonation and stabilizers of (otherwise unstable) azole carboxylic acid intermediates. A diverse azole substrate scope designed via machine learning-guided analysis demonstrates the broad utility of the sequence. DFT calculations provide insights into the role of silyl triflates in the reaction mechanism. Transferrable applications of the protocol are successfully established: (i) A low pressure (CO_2 balloon) option for synthesizing azole-2-carboxylic acids without the need for high-pressure equipment; (ii) the use of $^{13}CO_2$ for the synthesis of labeled compounds; and (iii) isocyanates as alternative electrophiles for direct C-H amidation. Fundamentally, the reported protocol expands the use of heterocycle C-H functionalization from late-stage functionalization applications towards its use in library synthesis. It provides general access to densely functionalized azole-2-carboxylic acid building blocks and demonstrates their one-pot use in diversifying amide couplings.

INTRODUCTION

C-H functionalization in drug development allows the use of unfunctionalized building blocks, enabling atom economical access to drug intermediates and active pharmaceutical ingredients (APIs).[1] With the prevalence of heterocyclic structures in biologically active compounds,[2] direct C-H functionalizations of heterocycles are of particular interest. However, as many bioactive heterocycles contain basic nitrogens, the formation of stable metal/heterocycle coordination complexes can inhibit metal catalysis; thus, establishing metal-catalyzed C-H functionalizations with broad functional group tolerance is often challenging.[3] Similarly, C-H functionalizations via deprotonation pathways applying strong bases and/or high reaction temperatures exhibit limited functional group tolerance due to forcing conditions.[4,5] As a result, advancing the mild and functional group tolerant C-H functionalizations of azoles[6-9] remains an important goal for synthetic development.

Azole-2-carboxylic acids are useful building blocks that can in principle be accessed via the C-H carboxylation of azoles;[10,11] amide couplings of such acids are a relatively straightforward way to access a vast array of desired chemical structures. However, only limited numbers of azole-2-carboxylic acids are commercially available, as illustrated in Scheme 1.[12] In contrast, the number of available azole parent compounds that could serve as substrates to access azole-2-carboxylic acids via C-H carboxylation is vast.

This difference in commercial availability is likely due to the limited stability of azole carboxylic acids, which suffer from decomposition via decarboxylation (the microscopic reverse of C-H carboxylation).[11,13] This issue could be addressed by developing mild and functional group tolerant conditions for C-H carboxylation, followed by *in-situ* amide bond formation or similar other functionalizations that produce stable compounds of interest.

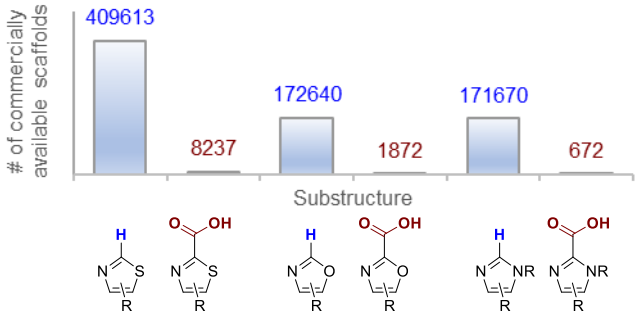

Scheme 1. Comparison of commercial availability of azole-H vs. azole-CO_2H building blocks.

Direct C-H carboxylations of 1,3-azoles have been reported previously (Scheme 2) in the presence of strong bases as additives. However, due to the above mentioned instability of azole carboxylic acids and the corresponding isolation challenges, the

obtained azole-2-carboxylic acids are most often reacted to obtain isolable esters.[10,11] Nevertheless, the combination of strong bases and/or high reaction temperatures limit the overall chemical space of azole-H scaffolds that can be employed under the reported conditions, thus not leveraging the full potential of azole C-H carboxylations. Therefore, we set out to establish azole C-H carboxylations under mild reaction conditions, to ultimately access a larger portion of the chemical space through expanding the use of amenable azole building blocks.

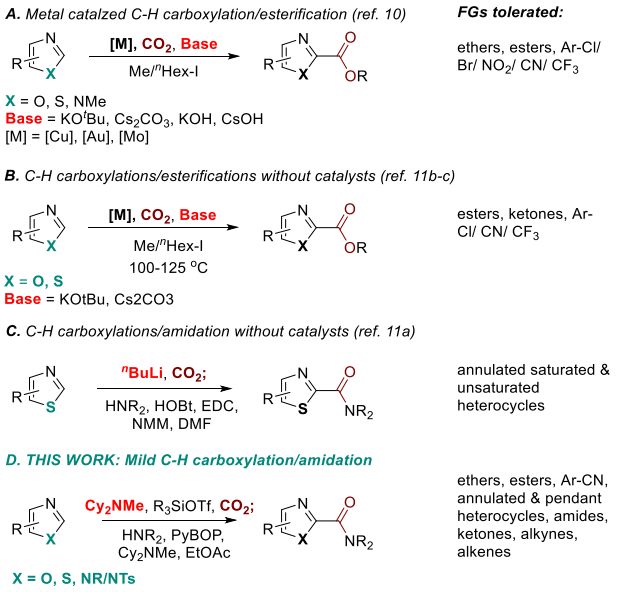

Scheme 2. Reported C-H carboxylations of azoles and work described herein. FGs = functional groups.

RESULTS AND DISCUSSION

We initially postulated that a recently reported, silyl-triflate mediated strategy for azole C-H aminoalkylation (Scheme 3)[14] may be transferrable to using CO_2 as electrophile. Since this strategy employs mild reaction conditions and bases, such a strategy could enable equally mild and functional group tolerant C-H carboxylations, allowing access of a broad range of azole carboxylic acids as building blocks.

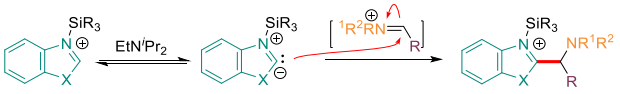

Scheme 3. Inspiration for mild C-H carboxylation: Silyl-triflate mediated C-H aminoalkylation.

HTE reaction optimization for C-H carboxylation. We began our investigations into establishing C-H carboxylations with a series of high-throughput experiments in which the effects of solvent, silyl triflate, base, CO_2 pressures, and reaction temperature were evaluated (for details, see the SI). Benzothiazole (**1**) was chosen as substrate for this campaign, as the product of C-H carboxylation (**2**) is commercially available; thus, the identity of the product can be unequivocally confirmed by comparison with the original material.

Excitingly, formation of the desired product **2** was observed in many of these experiments. Key results are shown in Scheme 4:

(i) Successful reactions contain both the amine base ($^{i}Pr_2NEt$) and a silyl triflate. (ii) A significant solvent dependence is observed, with ethereal solvents showing better reactivity. Among ethereal solvents, 1,2-dimethoxyethane (DME) is superior. (iii) TES-OTf results in slightly better reactivity than TBS-OTf or TMS-OTf, with TIPS-OTf being the least effective silyl triflate tested.

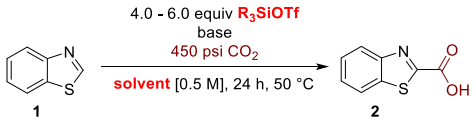

	None	TMSOTf [equiv]		TESOTf [equiv]		TIPSOTf [equiv]		TBSOTf [equiv]	
		4	6	4	6	4	6	4	6
DME	0	60	49	65	**71**	13	9	42	45
2-MeTHF	0	21	23	19	17	1	2	10	13
1,4-Dioxane	0	20	19	9	11	3	1	34	35
Toluene	0	26	22	11	15	7	6	2	2
MeCN	0	0	0	0	0	0	0	0	0
DMF	0	0	0	0	0	0	0	0	0
DCE	0	6	4	25	27	2	2	13	10
DMSO	0	0	6	0	0	0	2	1	2
	None	2 equiv $^{i}Pr_2NEt$							

Scheme 4. Selected HTE (high throughput experimentation) optimizations I: Influence of solvent, R_3SiOTf identity, and R_3SiOTf loading on product yield. Yields are color coded and shown as LCAP (Liquid Chromatography Area Percent) values. TMS = Me_3Si; TES = Et_3Si; TIPS = $^{i}Pr_3Si$; TBS = $^{t}BuMe_2Si$.

In a next step, we decided to further evaluate the loadings of the three successful silyl triflates, while also testing the influence of another bulky amine base, $NMeCy_2$ in addition to $^{i}Pr_2NEt$ (Scheme 5) at slightly lower CO_2 pressure (350 psi). Under these conditions, reactions with TMSOTf and TBSOTf perform well even at low silyl triflate loadings in the presence of 2 equiv of either $NMeCy_2$ or $^{i}Pr_2NEt$ as base. Reactions with TESOTf show their highest performance (94 LCAP product) at 6 equiv TESOTf and 2 equiv $MeNCy_2$.

In a next step, the concentration dependence (0.05 M to 2.0 M) of the reaction performance was evaluated (Scheme 6) using four high-yielding conditions identified previously (2 equiv TMSOTf/1.0 equiv $^{i}Pr_2NEt$; 5.0 equiv TESOTf/2.0 equiv $^{i}Pr_2NEt$; 5.0 equiv TESOTf/2.0 equiv $MeNCy_2$; and 2.0 equiv TBSOTf/2.0 equiv $^{i}Pr_2NEt$). The results show that only one silyl triflate (TESOTf) shows significant reactivity across all tested concentrations. Notably, this is true regardless of the amine base used (84 LCAP with $^{i}Pr_2NEt$; 92 LCAP with $NMeCy_2$ at 0.50 M). In contrast, TMSOTf/ $^{i}Pr_2NEt$ generally shows lower reactivity, while TBSOTf/ $^{i}Pr_2NEt$ only shows high reactivity under very dilute conditions (0.05 M). This suggests that TESOTf is the most reliable silyl triflate reagent for this transformation.

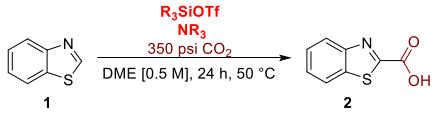

		iPr2NEt [equiv]			NMeCy2 [equiv]		
		0.5	1	2	0.5	1	2
TMSOTf [equiv]	1	20	32	85	10	27	66
	2	38	64	33	37	16	30
	6	40	79	73	29	51	51
TESOTf [equiv]	1	20	37	75	11	25	72
	2	34	63	31	31	41	59
	6	25	63	80	21	55	**94**
TBSOTf [equiv]	2	27	77	66	21	35	51
	6	23	61	78	33	60	80

Scheme 5. Selected HTE optimizations II: Influence of base and silyl triflate. Data are shown as LCAP of product 2.

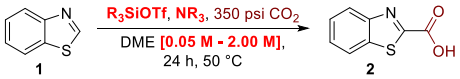

	0.05 M	0.1 M	0.25 M	0.5 M	1.0 M	2.0 M
2 equiv TMSOTf/ 1 equiv iPr2NEt	34	51	61	65	68	57
5 equiv TESOTf/ 2 equiv iPr2NEt	61	76	82	84	85	85
5 equiv TESOTf / 2 equiv NMeCy2	68	72	81	**92**	75	83
2 equiv TBSOTf/ 2 equiv iPr2NEt	81	79	54	63	34	25

Scheme 6. Selected HTE optimizations III: Concentration study. Data are shown as LCAP of product 2.

We suspected that the stability of the formed carboxylic acid (**2**) product could vary with the different reagent combinations used in screening. To test this hypothesis, the reaction mixtures obtained from the screen at 0.5 M (Scheme 6) were stored in the glovebox in vials with overpressure seals and the composition of the mixtures was monitored over time by UPLC (Scheme 7). Clearly, the LCAP (LC area percent) of **2** diminishes for some reagent mixtures, while no change is observed over >100 h for other reagent combinations. These data document stability differences that depend on the reagent combinations employed for C-H carboxylation: Reaction mixtures containing TESOTf (5 equiv) were stable, while reaction mixtures with TBSOTf (2 equiv) or TMSOTf (2 equiv) showed significant decomposition of **2**. These findings imply a correlation between silyl triflate loading and/or identity and azole-2-carboxylic acid stability.

These data and the literature[11,13] document that azole carboxylic acids often suffer from decomposition via decarboxylation. Nevertheless, accessing these intermediates in a functional group tolerant fashion is still impactful, if the follow-up coupling reactivity with other building blocks can be realized in a one-pot fashion. Since amide couplings are one of the key reactions in drug discovery that allow access to vast chemical space,[15] we decided to assess the feasibility of developing a C-H carboxylation-amide coupling reaction sequence in one pot.

HTE reaction optimization for amide coupling. When surveying literature conditions for amide couplings,[16] the use of polar aprotic solvents such as MeCN or DMF was common. However, such solvents are not compatible with the developed C-H carboxylation protocol (see Scheme 4 above). Therefore, we targeted the development of a one-pot, two-step protocol: the crude reaction mixture from C-H carboxylation would be diluted with a suitable solvent/reagent mixture for subsequent amidation. For reaction optimization, we employed HTE (Scheme 8) to evaluate 4 amide reagents (Figure 1), 6 solvents, and 4 bases for their ability to transform a crude solution of intermediate 2 into the desired amide product 4; benzylamine (3) was chosen as a coupling partner for initial experiments due to its abundance and ease of detection by UPLC(MS) analysis. To ensure an excess of polar aprotic solvent in the amide coupling step, we chose a solvent ratio of 1 : 4 (DME to polar aprotic solvent). Frequently used amide coupling reagents were evaluated, including HATU, COMU, and 2 reagents from the phosphonium reagent class (PyCloP, PyBoP).

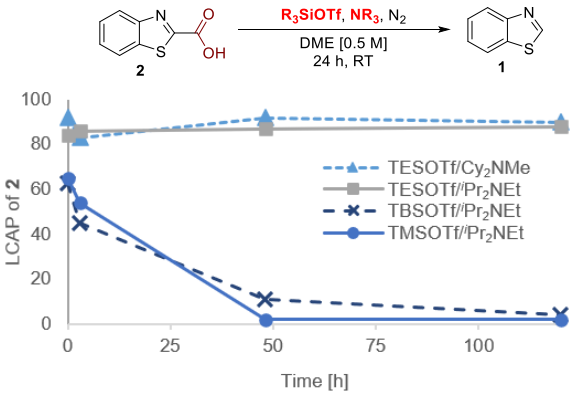

Scheme 7: Stability of 2 in crude reaction mixtures containing different silyl triflate/amine additives.

Interestingly, all amide coupling reagents formed the desired product **4** in all reactions, demonstrating the typical robustness of amide couplings and that a one-pot, two-step protocol for C-H carboxylation/amide coupling is feasible. The data also show that PyCloP and PyBOP are superior to HATU and COMU in this case: reactions containing $NMeCy_2$ as base and EtOAc as reaction solvent afforded up to 78% AY (assay yield; Scheme 8A).

A follow-up HTE experiment (for more reaction optimization, see the SI) evaluated PyCloP and PyBOP in combination with different solvents and base loadings (Scheme 8B). The best HTE results (1.0 equiv $BnNH_2$ **3**, 1.1 equiv PyBOP, 4 equiv $MeNCy_2$) were verified at a reaction scale of 2.5 mmol, affording **4** in 86% AY (Scheme 9).

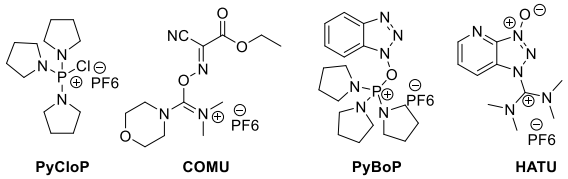

Figure 1. Evaluated amine coupling reagents.

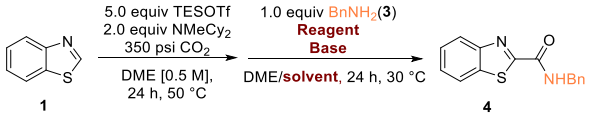

A. Parallel evaluation of base, solvent, and coupling reagent.

	MeCN	2-MeTHF	EtOAc	MeCN	2-MeTHF	EtOAc
	PyCloP			HATU		
$^{i}Pr_2NEt$	34	32	50	27	36	24
NMM	36	24	61	17	48	48
$NMeCy_2$	16	26	**68**	16	29	20
NEt_3	33	27	46	18	8	36
	COMU			PyBoP		
$^{i}Pr_2NEt$	48	24	12	58	27	73
NMM	22	34	30	42	28	74
$NMeCy_2$	4	23	15	45	30	**78**
NEt_3	15	22	9	41	19	60

B. Parallel evaluation of base loading, solvent, and coupling reagent.

	$^{i}Pr_2NEt$ [equiv]			$NMeCy_2$ [equiv]			
	2.0	3.0	4.0	2.0	3.0	4.0	
MeCN	42	47	35	46	36	34	PyCloP
EtOAc	24	57	61	39	58	65	
IPAC	23	45	49	34	48	49	
NMP	2	14	16	4	13	14	
MeCN	27	49	51	26	48	47	PyBOP
EtOAc	7	53	**86**	40	75	**87**	
IPAC	1	49	43	21	68	70	
NMP	0	23	38	2	35	34	

Scheme 8. AYs for selected amide coupling optimizations.

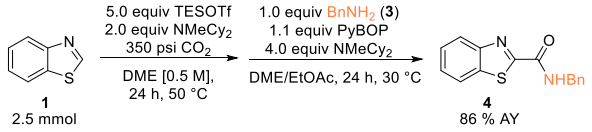

Scheme 9. Confirmation of HTE optimization results *via* scale-up.

Azole substrate scope via machine-learning guided chemical space analysis. With the optimized one-pot, two-step conditions in hand, we next focused on exploring the azole substrate scope. As shown in Scheme 1, the number of commercially available 1,3-azole substrates is vast. Therefore, we decided to employ unsupervised machine learning to analyze the structural diversity of available substrates. Specifically, over 16,000 azole substrates were featurized into molecular descriptors available on RDKit.[17] Principal component analysis (PCA) was used to extract important features and reconstruct the data into principal components. t-distributed stochastic neighbor embedding (t-SNE)[18] was implemented to visualize the high-dimensional data (Scheme 10). In contrast to the "classical" approach to substrate scopes (use of simple substrates, systematic variation of electronic and steric parameters), this approach allows the choice of substrates representative of the complete chemical space to be surveyed.[19] Clustering of similar chemical matter ensured that substrates from each relevant area of the chemical space would be chosen and tested.

For selection of azole substrates, several criteria were applied: (i) Inclusion of substructures that would likely not undergo azole C-H carboxylations under previously known conditions (strong bases, high temperatures);[10,11] (ii) Limited commercial availability for the majority of the corresponding azole carboxylic acid products: out of the chosen substrates, 17 carboxylic acids are not commercially available; 9 scaffolds show less than 5 vendors in a SciFinder search. (iii) Evaluate similar numbers of oxazoles (12), thiazoles (10), and imidazoles (17), even though imidazoles take up a significantly larger portion of the chemical space map than oxazoles and thiazoles. (iv) Ready commercial availability on gram scale, *i.e.* more than 5 vendors in SciFinder or gram-scale availability in our internal compound collection.

With these guiding principles in mind, we used the chemical space map in Scheme 10 to identify 39 representative azole scaffolds. These substrates were subjected to the one-pot C-H carboxylation/amide coupling conditions that had been optimized for the synthesis of **4** (Scheme 11); all products were synthesized in reaction arrays, using parallel synthesis workflows. The obtained AYs (determined by quantitative NMR analysis of crude reaction mixtures) and isolated yields are provided for each substrate in Scheme 11 to reflect both the inherent reactivity of an azole and the ease of isolation.

Excitingly, 32 of the 39 chosen substrates were successfully reacted to obtain the corresponding azole-2-amides. These include (benz)oxazoles, (benzo)thiazoles, and (benz)imidazoles. Various functionalities such as ethers (**11**), ketones (**16**, **21**, **25**), amides (**14**, **24**), esters (**13**, **15**, **22**), alkenes (**10**, **22**, **32**), alkynes (**23**), nitriles (**12**) and additional heterocyclic substructures (**7**, **14**, **18**, **30**, **31**, **33**, **34**) are well tolerated under the mild reaction conditions.

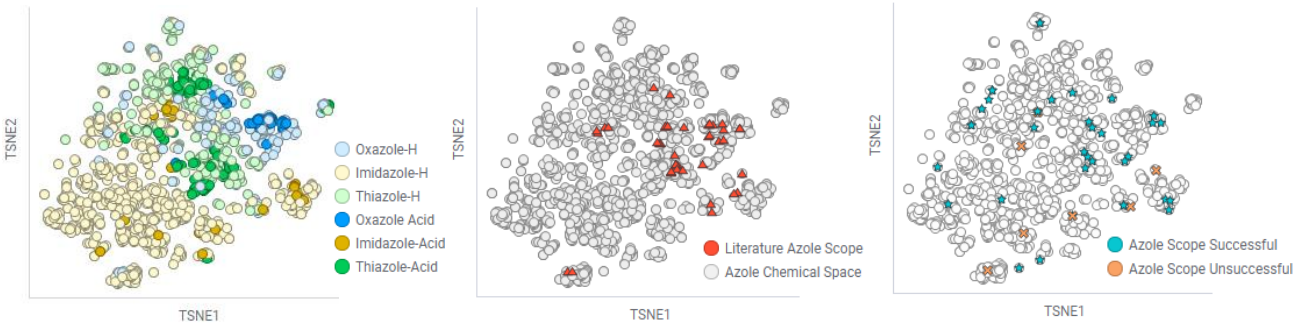

Scheme 10. Chemical space map of azole scaffolds. The scaffolds included in this analysis include building blocks in our internal building block collection and from commercially available sources (*e.g.*, Enamine).

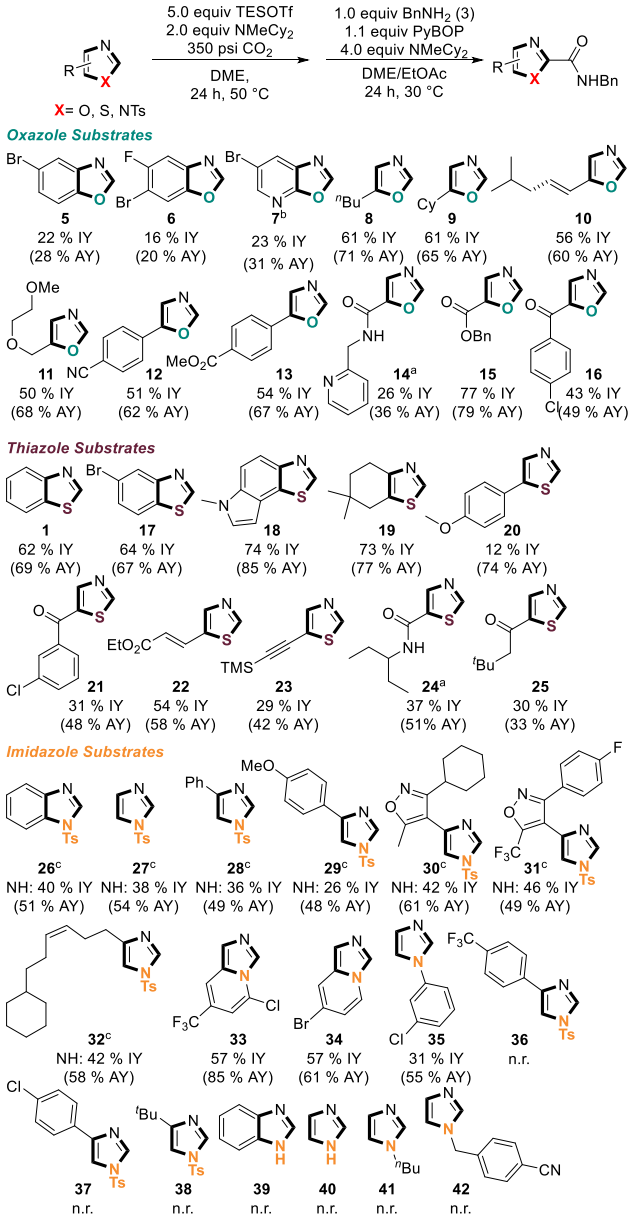

Scheme 11. Azole substrate scope. IY= isolated yield. AY = assay yield. Products were synthesized using parallel synthesis workflows. [a]Modification for substrates with acidic CH or NH bonds: TESOTf (6.0 equiv), $NMeCy_2$ (3.0 equiv) in step 1vand $NMeCy_2$ (5.0 equiv) in step 2. [b]Modification: TBSOTf (4.0 equiv), $^{i}Pr_2NEt$ (3.0 equiv) in step 1 and $^{i}Pr_2NEt$ (4.0 equiv) in step 2. [b]Detosylative workup: pyridine/water (4:1), 50 °C, 5 h.

All tested oxazoles and thiazoles showed significant product formation. In contrast, protection (and acidification) with a Ts group is necessary for most imidazoles to enable sufficient C-H functionalization reactivity: Both benzimidazole (**39**) and imidazole (**40**) do not show any reactivity, but their tosylated analogues **26** and **27** readily undergo the desired reactivity to afford 51% and 54% AY, respectively. Interestingly, such activation via acidification is not necessary for *N*-aryl (**35**) or annulated imidazoles (**33**, **34**). Imidazole scaffolds containing *N*-alkyl substructures (**41**, **42**) and 4-substituted N-tosyl imidazoles (**36**, **37**, **38**) did not form desired products.

Amine Scope. To evaluate the scope of amines, 12 amine substrates were selected and reacted in parallel under the previously optimized conditions. For all these reactions, thiazole (**1**) was employed as azole coupling partner. As shown in Scheme 12, 11 of the 12 employed amine building blocks were successfully reacted, with **53** being the only amine showing no formation of desired product. Notably, the mild reaction sequence allows access to Weinreb amides by employing **47** as coupling partner; the obtained amide product can serve as a valuable building block for further late-stage diversification.[20]

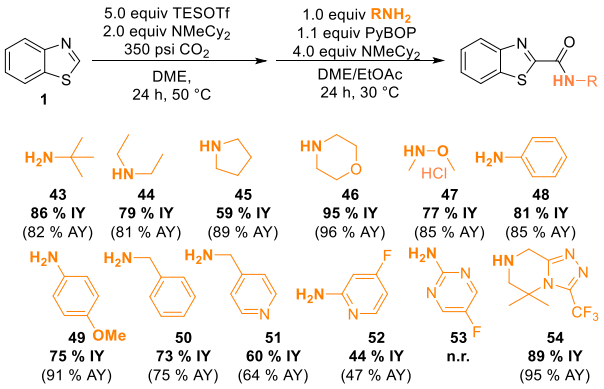

Scheme 12. Amine scope. Products were synthesized using parallel synthesis workflows.

Mechanistic analysis and discussion. Having established azole C-H carboxylations/amidations under mild reaction conditions, we turned our attention towards understanding key questions regarding the reaction mechanism: What is the role of the silyl triflate additive? How does CO_2 act with reaction intermediates to form a new C-C bond? Can the azole substrate scope aid with predicting reactivity of diverse azoles? Both experimental and computational tools were employed to gain insight into these questions.

Role of R_3SiOTf for C-H deprotonation. Based on our previous work in C-H aminoalkylation,[14] we hypothesized that one of the roles of the silyl triflate would be to activate the azole for deprotonation via silylation. Indeed, silyl-adducts of azoles (**55-58**; Scheme 13) can be identified by UPLC/MS in C-H carboxylation reaction mixtures (see SI for detailed MS spectra), suggesting that such adducts have significant stability.

DFT calculations support the intermediacy of *N*-silylated intermediates as a likely pathway: Deprotonation of *N*-silylated thiazole **1-TMS** (ΔG = +11.5 kcal/mol; Scheme 14) is significantly lower in energy than the corresponding deprotonation of thiazole (**1**) without prior silylation (ΔG = +31.3 kcal/mol).

Another role of silyl triflates could be to activate CO_2 and thus increase its electrophilicity and/or availability in solution. To test this hypothesis, DFT calculations on the equilibrium between CO_2 and TMSOTf to the corresponding adduct were performed. The results of these calculations (ΔG = +42.6 kcal/mol; Scheme 15) indicate that CO_2 and TMSOTf are unlikely to form an adduct under the conditions for C-H carboxylation.

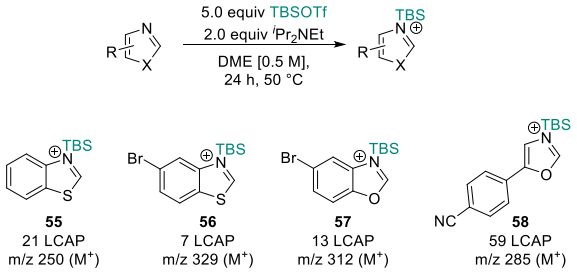

Scheme 13. Identification of azole-TBS adducts by UPLC/MS analysis.

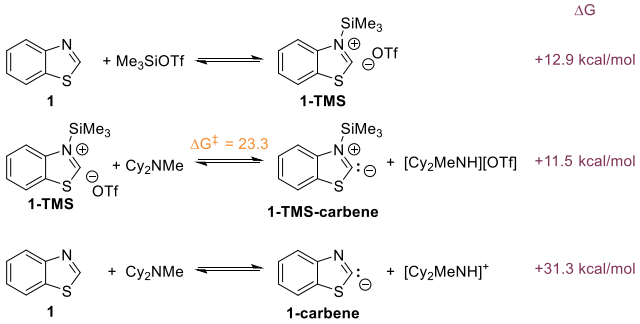

Scheme 14. Comparison of deprotonation equilibria with and without *N*-silylation. See SI for details of computational methods. M06-2X/def2TZVPP/SMD(ether)//M06-2X/6-31G(d)/SMD(ether)

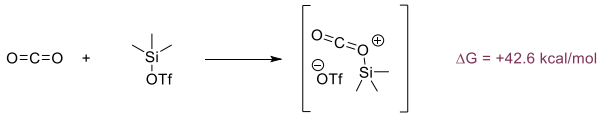

Scheme 15. Free enthalpy of adduct formation between CO_2 and TMSOTf. M06-2X/def2TZVPP/SMD(ether)//M06-2X/6-31G(d)/SMD(ether)

***CO_2 insertion*.** Having established that silyl triflates activate the azole substrate for deprotonation *via N*-silylation, it seems logical to assume that the electrophile CO_2 would react with the nucleophilic **1-TMS-carbene** to form a new C-C bond. To test if the carboxylation step may be rate-determining in the C-H carboxylation of **1**, we performed a series of rate studies at different temperatures and pressures (see Scheme 16). Interestingly, both increased temperature (RT vs. 50 °C) and increased CO_2 pressure (350 psi vs. 14.6 psi) result in an increase in reaction rate. These data suggest that CO_2 is involved in the reaction mechanism at or before the rate-determining step of C-H carboxylation.

DFT calculations were again employed to shed more light on this possibility. The results of the calculations (Scheme 17) show that CO_2 insertion is indeed the rate-determining step of the reaction ($\Delta G^{\ddagger}$ = 24.8 kcal/mol), while the deprotonation barrier is only slight lower ($\Delta G^{\ddagger}$ = +23.3 kcal/mol). Notably, the silyl group helps to stabilize the transition state **TS2** via electrostatic interactions with the developing negative electron density at the oxygen of CO_2.The silyl group also stabilizes the insertion product **1-TMS-CO2** via formation of a pentavalent Si center.

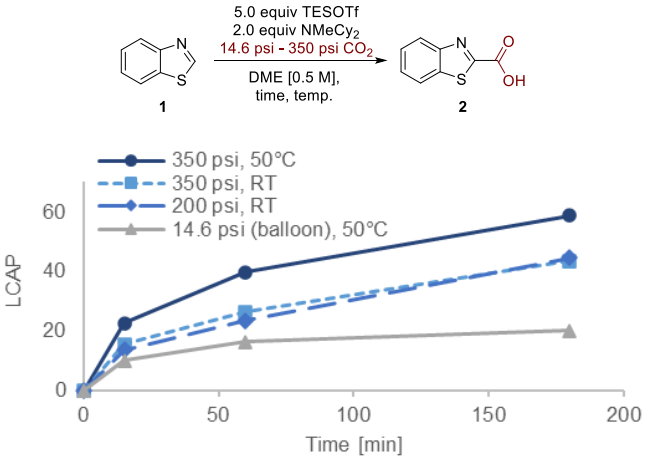

Scheme 16: C-H carboxylation reaction profile at varying CO_2 pressure and temperature.

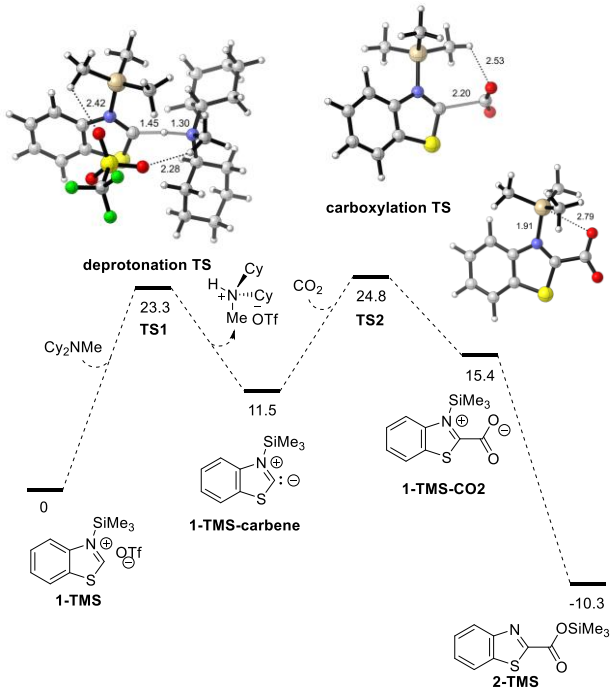

Scheme 17. Energy landscape and transition state structure for C-H carboxylation. M06-2X/def2TZVPP/SMD(ether)//M06-2X/6-31G(d)/SMD(ether)

Stabilization of azole carboxylic acid products. Based on the previously documented stability differences of **2** in the presence of different silyl triflates (see Scheme 7 above), we postulated that another role of silyl triflates may be to stabilize the C-H carboxylation product. In order to experimentally characterize the species formed when reacting an azole-2-carboxylic acid with silyl triflates, **2** was reacted with TESOTf in MeCN-D_3. ^{13}C NMR analysis of this solution revealed a clear shift of the two silyl triflate signals from 5.96 ppm to 6.62 ppm and from 5.36 ppm to 5.05 ppm, respectively (Scheme 18; for further details, see SI). This suggests that silylation of **2** is rapid; this is also supported by the observation that the initial suspension of **2** in MeCN-D_3 transforms into a clear solution immediately

after addition of TESOTf. The formation of a silyl ester as intermediate is further supported by DFT (see Scheme 19); interestingly, silyl group migration (from **1-TMS-CO2** to **2-TMS**) through a penta-coordinated silicate transition state/intermediate is preferred over a silylation/desilylation pathway.

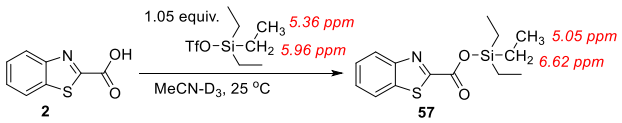

Scheme 18. Detection of silyl ester by ^{13}C NMR analysis. ^{13}C NMR shifts are depicted in red italic font.

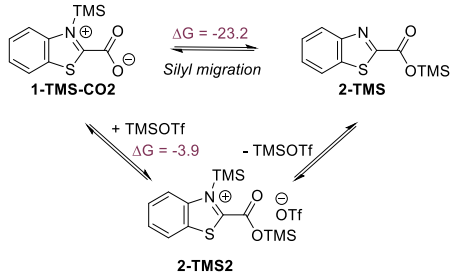

Scheme 19. Free energy landscape for silyl ester formation after CH carboxylation. M06-2X/def2TZVPP/SMD(ether)//M06-2X/6-31G(d)/SMD(ether)

In summary, these data suggest three distinct roles for silyl triflates in C-H carboxylation: (1) Silyl triflate coordination acidifies the azole C_2-H position, which makes the azole substrate amenable to deprotonation by a mild amine base. (2) The silyl triflate group aids in stabilizing the carboxylation transition state (**TS2**) and the direct product of C-H carboxylation (**1-TMS-CO2**). (3) Silyl triflates react with azole carboxylic acids to form a silyl ester, thus stabilizing carboxylic acid intermediates that may otherwise decompose via decarboxylation.

Analysis of azole scope data. We then turned our attention to documenting reactivity trends across the tested azoles substrates. Since we had used a chemical space map to ensure the selection of diverse substrates, we reasoned that the obtained data set would allow us to assess trends across the relevant azole space. First, to validate the use of AYs in our analysis, we correlated amidation AYs with IYs (see Scheme 20A). This analysis shows that AYs determined by quantitative ^{1}H NMR using an internal standard and IYs correlate well with only one significant outlier. This suggested that the use of AY data is useful for further analysis, especially since AYs are typically a better measure of reaction success than IYs, which can depend on the recovery during workup and isolation.

Considering the potential instability of carboxylic acid intermediates, we were curious if the C-H carboxylation reactivity (noted in LCAP of the carboxylic acid intermediate) would also correlate with the AY of amide product; those data are visualized in Scheme 20B. Interestingly, for many azole substrates, there seems to be a correlation; however, many substrates show a lower LCAP of carboxylic acid intermediate than what would be expected based on the obtained assay yield of amide product.

This suggests that a high LCAP of azole carboxylic acid is a good predictor of high conversion to the amide product. The opposite, however, is not true: A low LCAP of azole carboxylic acid may not necessarily mean that the subsequent amide product cannot be formed. These data may most easily be explained by the consideration that azole carboxylic acids are not always stable under UPLC/MS conditions; thus, low LCAPs may not mean that azole carboxylic acids have not been formed efficiently, but that the specific azole carboxylic acid is not very stable under the conditions of UPLC/MS analysis.

For the next step of our analysis, the free energies of deprotonation for each azole substrate for deprotonation at C_2-H with Cy_2NMe ($\Delta G_{deprotonation}$) after *N*-silylation were calculated (Scheme 20E); those values were then plotted again both the LCAP of C-H carboxylation product (Scheme 20C) and the AY of amide product (Scheme 20D). No correlation is observed between $\Delta G_{deprotonation}$ and the LCAP of C-H carboxylation product (Scheme 20C). Likely, this lack of a correlation reflects that carboxylation has a higher barrier than C-H deprotonation and occurs after deprotonation in the proposed reaction mechanism (see Scheme 17 above). Another reason for the lack of correlation could be the varying instability of azole-carboxylic acids under UPLC/MS conditions (see discussion of Scheme 20B).

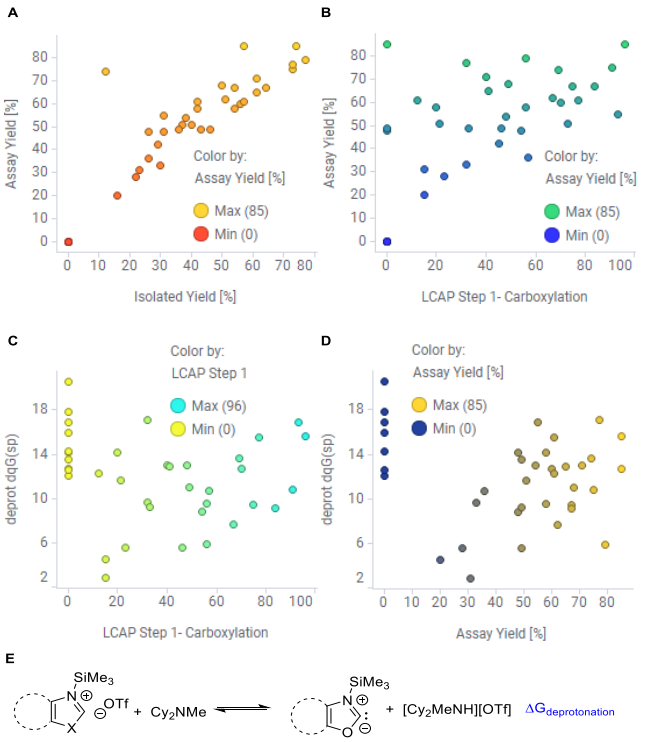

Scheme 20. Azole scope data analysis. A. AY vs. IY. B. LCAP of C-H carboxylation vs. AY of amidation. C. $\Delta G_{deprotonation}$ vs. LCAP of C-H carboxylation. D. $\Delta G_{deprotonation}$ vs. AY. E. Deprotonation equilibrium used to determine $\Delta G_{deprotonation}$.

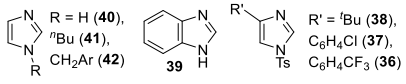

Figure 2. Azole substrates that do not convert to desired C-H amidation product.

When correlating $\Delta G_{deprotonation}$ and the AYs of amide product (Scheme 20D), the data split into two reactivity regimes: The

first set of substrates includes those that do not convert to the desired products at all; those data points are clustered in the top left corner of the plot. Those substrates are shown Figure 2 and likely do not undergo C-H carboxylation under the reaction conditions. The reasons for their unreactivity likely range from steric bulk preventing *N*-silylation/deprotonation to insufficient C-H acidity.

The substrates in the second regime (right side of Scheme 20D) show a loose correlation between $\Delta G_{deprotonation}$ and the AY of the corresponding amide product: The more stable the *N*-silylated carbene intermediate, the lower the obtained AYs. This seems at first counterintuitive, since azole deprotonation is the first step in the reaction mechanism, preceding C-C bond formation. However, this correlation may point to the importance of another step in the overall reaction: stable carbene intermediates are likely correlated with facile decarboxylation of azole-2-carboxylic acids under the conditions of amide bond formation. Therefore, the stability of azole carboxylic acids against decarboxylation is a precondition for high yields of amide products. Scheme 21 illustrates this trend with 3 examples from the substrate scope: more favorable decarboxylation of the *N*-silylated intermediate (forming the N-silylated carbene) are correlated with lower AYs of amide product.

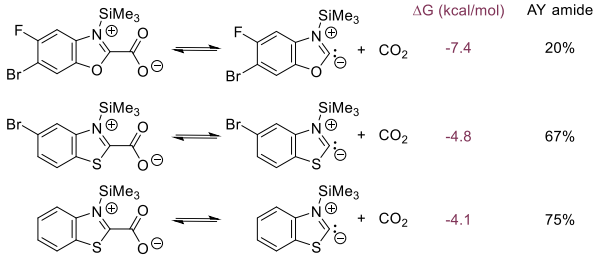

Scheme 21. Decarboxylation equilibria. M06-2X/def2TZVPP/SMD(ether)//M06-2X/6-31G(d)/SMD(ether)

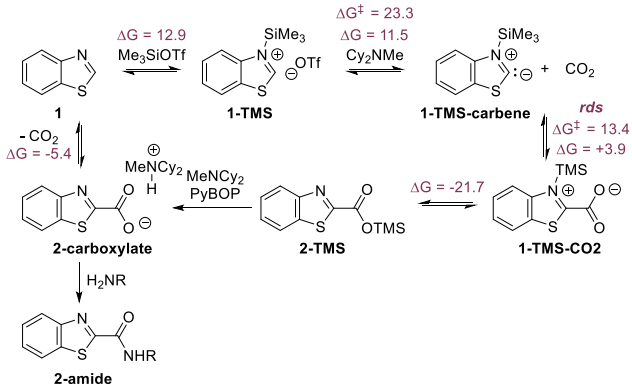

Scheme 22. Proposed mechanism. Energies are shown in kcal/mol.

Conclusions from mechanistic studies & data analysis. Overall, the studies summarized in this section highlight the importance of silyl triflate additives for all steps of the C-H carboxylation mechanism. Furthermore, the use of yield data obtained across a broad spectrum of azole substrates highlights the importance of considering the stability of the azole-2-carboxylic acid intermediate for overall reaction success. This analysis provides a loose correlation between the thermodynamics of decarboxylation and the stability of the silylated carbene intermediates. Scheme 22 summarizes the proposed mechanism for the developed transformation and includes the free energies for each elementary step in the reaction profile.

Transferrable applications. Having developed a thorough understanding of the one-pot C-H carboxylation/amidation sequence, we wanted to further expand the utility of the protocol. We thus chose to demonstrate (i) that the reaction can be used without the need for high-pressure equipment; (ii) that $^{13}CO_2$ can be employed as electrophile to access labeled compounds; and (iii) that other heterocumulenes than CO_2 show analogous reactivity.

Reactions under low CO_2 pressure. We considered that high-pressure reactors are not always available; therefore, a "low pressure option" of the protocol could be amenable for implementation outside of specialized facilities. We thus decided to test if the reaction can be performed in commonly available reactors. To realize such conditions, we conducted the reaction sequence in a microwave vial equipped with a CO_2 filled balloon (14.6 psi CO_2 pressure; Scheme 23). Notably, 50 LCAP of carboxylic acid **2** was observed after 24 h. The crude reaction mixture was then reacted with the amide coupling solvent/reagent mix developed above. To our delight, this setup afforded 39% AY of desired product **4**, illustrating that the developed one-pot, two-step reaction sequence can be executed without a gas manifold, albeit with loss of product yield.

Incorporation of ^{13}C using $^{13}CO_2$ as reactant. Introducing isotopic labels (^{13}C and ^{14}C) into organic molecules with biological activity is crucial to enable drug metabolism, drug deposition and/or pharmacokinetic (DMPK) studies.[21] $^{13}CO_2$ is a common surrogate for $^{14}CO_2$ and $^{11}CO_2$ and often utilized for the development of isotopic exchange reactions.[22] To illustrate that the developed procedure would support such labeling studies, we demonstrated the synthesis of **^{13}C-4** on a 250 mg scale (Scheme 24); the desired compound was obtained in 34% IY.

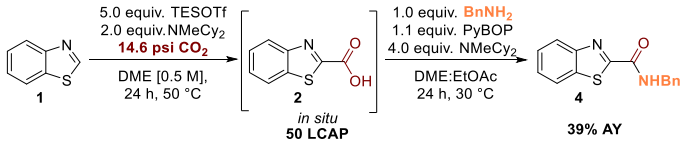

Scheme 23. C-H carboxylation/amidation sequence in one-pot with CO_2 balloon.

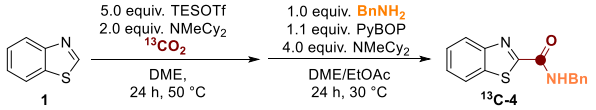

Scheme 24. Synthesis of ^{13}C-labeled azole amide ^{13}C-4.

Direct C-H amidation with isocyanates as electrophiles. Inspired by our success using CO_2 as electrophile, we speculated that other heterocumulenes such as isocyanates may show similar reactivity due to their comparable electrophilicity.[23,24] Indeed, a multidimensional reaction optimization via HTE (see SI for details) demonstrated that such one-step C-H amidation reactivity can be established. The reactivity of isocyanates in this reaction depends closely on their electronic nature: aromatic isocyanates (**59**-**61**) show greater reactivity than aliphatic

isocyanates (**62**, **63**) (Scheme 25). Those observations correlate with observations in the literature, in which only aromatic isocyanates illustrated reactivity.[23a]

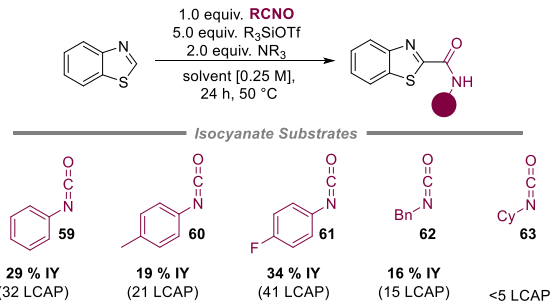

Scheme 25. Silyl triflate mediated C-H amidation with isocyanate electrophiles.

SUMMARY AND CONCLUSIONS

Overall, this manuscript details the development of mild and functional group tolerant azole C-H carboxylation/amidation conditions. This transformation significantly expands the chemical space of accessible azole-2-amides. The azole substrate scope thus demonstrates the synthesis of diverse, previously inaccessible products. Relying on a chemical space map established by unsupervised machine learning enables the selection of representative substrates. Detailed mechanistic investigations employing both experimental and computational methods allow insights into the factors governing the success of the transformation and provide information on the key steps of the reaction mechanism. Importantly, these studies identify one key predictor of success for C-H carboxylation/amidation: the stability of the azole carboxylic acid intermediate. Finally, transferrable applications of these learnings are successfully established: a low pressure (CO_2 balloon) option; the use of $^{13}CO_2$; and employing isocyanates as alternative electrophiles for direct C-H amidation.

We expect that these developments will allow the broader application of C-H functionalization methods for the synthesis of biologically active molecules beyond applications in late-stage functionalization settings. Particularly, the demonstrated methodology allows the construction of key amide bonds in heterocyclic structures. Furthermore, it enables the incorporation of a novel set of commercially available, 1,3-azole building blocks through providing highly functional group tolerant C-H functionalization conditions, thus allowing access to diverse chemical matter.

ASSOCIATED CONTENT

Supporting Information

The Supporting Information is available free of charge at pubs.acs.org. Experimental procedures for all reactions; spectroscopic characterization data for all new compounds and copies of ^{1}H- and ^{13}C- NMR Spectra (PDF)

AUTHOR INFORMATION

Corresponding Authors

*__Marion H. Emmert__; https://orcid.org/0000-0003-4375-8295; Email: marion.emmert@merck.com

*__Cyndi Q. He__; https://orcid.org/0000-0002-3143-6435; E-mail: cyndi.he@merck.com

*__Stephanie Felten__; https://orcid.org/0000-0002-5477-5026; Email: stephanie.felten@merck.com

Author Contributions

$ M.H.E. and S.F. conceptualized the project. S.F., M.S. and M.W. performed experiments. C.Q.H. performed computations. S.F., C.Q.H., and M.H.E. wrote the manuscript and performed data analysis. All authors have given approval to the final version of the manuscript.

Notes

The authors declare no competing financial interest.

ACKNOWLEDGMENT

The authors acknowledge Michael T. Pirnot, Akshay A. Shah, Anthony Shaw, Rebecca Ruck, and Neil Strotman (all Merck & Co., Inc., Rahway, NJ, USA) for insightful discussions. We thank Christopher Nietupski and Michael Whittington (Merck) for experimental assistance. We acknowledge Rodell Barrientos (Merck) for assistance with HRMS measurement.

REFERENCES

(1) Selected reviews on C–H activation/functionalizations, see: (a) Wencel-Delord, J.; Dröge, T.; Liu, F.; Glorius, F., Towards Mild Metal-Catalyzed C−H Bond Activation. *Chem. Soc. Rev.* **2011**, *40*, 4740−4761. (b) Gensch, T.; Hopkinson, M. N.; Glorius, F.; Wencel-Delord J., Mild Metal-Catalyzed C−H Activation: Examples and Concepts. *Chem. Soc. Rev.* **2016**, *45*, 2900−2936. (c) Davies, H. M. L.; Morton D., Collective Approach to Advancing C−H Functionalization. *ACS Cent. Sci.* **2017**, *3*, 936−943. (d) Sambiagio, C.; Schönbauer, D.; Blieck, R.; Dao-Huy, T.; Pototschnig, G.; Schaaf, P.; Wiesinger, T.; Farooq Zia, M.; Wencel-Delord, J.; Besset, T.; Maes, B. U. W.; Schnürch M., A Comprehensive Overview of Directing Groups applied in metal-catalysed C–H functionalisation chemistry. *Chem. Soc. Rev.* **2018**, *47*, 6603–6743. (e) Gandeepan, P.; Müller, T.; Zell, D.; Cera, G.; Warratz, S.; Ackermann L., 3d Transition Metals for C−H Activation. *Chem. Rev.* **2019**, *119*, 2192−2452. (f) Kaur, M.; Van Humbeck, J. F., Recent trends in catalytic sp^3 C–H functionalization of heterocycles. *Org. Biomol. Chem*., **2020**, *18*, 606–617. (g) Dalton, T.; Faber, T.; Glorius F., C−H Activation: Toward Sustainability and Applications. *ACS Cent. Sci.* **2021**, *7*, 245−261. (h) Guillemard, L.; Kaplaneris, N.; Ackermann, L.; Johansson, M. J., Late-stage C–H functionalization offers new opportunities in drug discovery. *Nat. Rev. Chem.* **2021**, *5*, 522-546. (i) Rogge, T.; Kaplaneris, N.; Chatani, N.; Kim, J.; Chang, S.; Punji, B.; Schafer, L. L.; Musaev, D. G.; Wencel-Delord, J.; Roberts, C. A.; Sarpong, R.; Wilson, Z. E.; Brimble, M. A.; Johansson, M. J.; Ackermann, L., C–H activation. *Nat. Rev. Methods Primers* **2021**, *1*, 43-74. (j) Grover, J.; Prakash, G.; Goswami, N.; Maiti, D., Traditional and sustainable approaches for the construction of C–C bonds by harnessing C–H arylation. *Nat. Commun.* **2022**, *13*, 1085- 1102.

(2) (a) Vitaku, E.; Smith, D. T.; Njardarson, J. T., Analysis of the Structural Diversity, Substitution Patterns, and Frequency of Nitrogen Heterocycles among U.S. FDA Approved Pharmaceuticals. *J. Med. Chem.* **2014**, *57*, 10257−10274. (b) Kerru, N.; Gummidi, L.; Maddila, S.; Kumar Gangu, K.; Jonnalagadda, S. B., Review on Recent Advances in Nitrogen-Containing Molecules and Their Biological Applications. *Molecules* **2020**, *25* (8), 1909-1951.

(3) Das, R.; Kapur, M., Transition-Metal-Catalyzed C−H Functionalization Reactions of π-Deficient Heterocycles. *Asian J. Org. Chem.* **2018,** *7* (7), 1217-1235.

(4) a) Do, H.-Q.; Khan, R. M. K.; Daugulis, O., A General Method for Copper-Catalyzed Arylation of Arene C-H Bonds. *J. Am. Chem. Soc*. **2008**, *130*, 15185–15192. (b) Cho, S. H.; Kim, J. Y.; Kwak, J.; Chang, S., Recent advances in the transition metal-catalyzed two fold oxidative C–H bond activation strategy for C–C and C–N bond formation. *Chem. Soc. Rev*. **2011**, *40*, 5068–5083.

(5) Selected reviews on azole C-H functionalizations, see: (a) Basak, S.; Dutta, S.; Maiti, D., Accessing C2-Functionalized 1,3-(Benz)azoles through Transition Metal-Catalyzed C-H Activation. *Chem. Eur. J*. **2021**, *27*, 10533 – 10557 (b) Chen, S.; Ranjan, P.; Voskressensky, L. G.; Van der Eycken, E. V.; Sharma, U. K., Recent Developments in Transition-Metal Catalyzed Direct C–H Alkenylation, Alkylation, and Alkynylation of Azoles. *Molecules* **2020**, *25*, 4970-5004. (c) Arora, A.; Weaver, J. D., Visible Light Photocatalysis for the Generation and Use of Reactive Azolyl and Polyfluoroaryl Intermediates. *Acc. Chem. Res.* **2016**, *49*, 2273−2283.

(6) Selected examples of Ni-catalyzed azole C−H functionalizations, see: (a) Amaike, K.; Muto, K.; Yamaguchi, J.; Itami, K., Decarbonylative C–H Coupling of Azoles and Aryl Esters: Unprecedented Nickel Catalysis and Application to the Synthesis of Muscoride A. *J. Am. Chem. Soc*., **2012**, *134*, 13573-13576; (b) Muto, K.; Yamaguchi, J.; Itami, K., Nickel-Catalyzed C–H/C–O Coupling of Azoles with Phenol Derivatives. *J. Am. Chem. Soc*., **2012**, *134*, 169-172; (c) Yamamoto, T.; Muto, K.; Komiyama, M.; Canivet, J.; Yamaguchi, J.; Itami, K., Nickel-Catalyzed C−H Arylation of Azoles with Haloarenes: Scope, Mechanism, and Applications to the Synthesis of Bioactive Molecules. *Chem.–Eur. J*., **2011**, *17*, 10113-10122; (d) Meng, L.; Kamada, Y.; Muto, K.; Yamaguchi, J.; Itami, K., C−H Alkenylation of Azoles with Enols and Esters by Nickel Catalysis. *Angew. Chem., Int. Ed*., **2013**, *52*, 10232-10235; (e) Xu, H.; Muto, K.; Yamaguchi, J.; Zhao, C.; Itami, K.; Musaev, D. G., Key Mechanistic Features of Ni-Catalyzed C–H/C–O Biaryl Coupling of Azoles and Naphthalen-2-yl Pivalates. *J. Am. Chem. Soc*., **2014**, *136*, 14834-14844; (f) Larson, H.; Schultz, D.; Kalyani, D., Ni-Catalyzed C−H Arylation of Oxazoles and Benzoxazoles Using Pharmaceutically Relevant Aryl Chlorides and Bromides. *J. Org. Chem.*, **2019**, *84*, 13092-13103. (g) Hanson, M. G.; Olson, N. M.; Yi, Z.; Wilson, G.; Kalyani, D., Nickel-Catalyzed Coupling of Azoles with Aromatic Nitriles. *Org. Lett.* **2017,** *19* (16), 4271-4274.

(7) Selected examples of Cu-catalyzed azole C−H functionalizations, see: (a) Do, H.-Q.; Daugulis, O., Copper-Catalyzed Arylation of Heterocycle C−H Bonds. *J. Am. Chem. Soc*. **2007**, *129*, 12404- 12405 (b) Yoshizumi, T.; Tsurugi, H.; Satoh, T.; Miura, M., Copper-mediated direct arylation of benzoazoles with aryl iodides. *Tetrahedron Lett*. **2008**, *49*, 1598; (c) Nishino, M.; Hirano, K.; Satoh, T.; Miura, M., Copper-Mediated and Copper-Catalyzed Cross-Coupling of Indolesand 1,3-Azoles: Double C−H Activation. *Angew. Chem., Int. Ed*. **2012**, *51*, 6993-6997; (d) Ohmiya, H.; Zhang, H.; Shibata, S.; Harada, A.; Sawamura, M., Construction of Quaternary Stereogenic Carbon Centers through Copper-Catalyzed Enantioselective Allylic Alkylation of Azoles. *Angew. Chem., Int. Ed*., **2016**, *55*, 4777-4780.; (e) Gandeepan, P.; Mo, J.; Ackermann, L., Photo-induced copper-catalyzed C–H chalcogenation of azoles at room temperature. *Chem. Commun*. **2017**, *53*, 5906-5906. (f) Armstrong, A.; Collins, J. C., Direct Azole Amination: C−H Functionalization as a New Approach to Biologically Important Heterocycles. *Angew. Chem. Int. Ed*. **2010**, *49*, 2282 – 2285.

(8) Selected examples of Pd-catalyzed azole C−H functionalizations, see: (a) Campeau, L.-C.; Bertrand-Laperle, M.; Leclerc, J.-P.; Villemure, E.; Gorelsky, S.; Fagnou, K., C2, C5, and C4 Azole *N*-Oxide Direct Arylation Including Room-Temperature Reactions. *J. Am. Chem. Soc.* **2008**, *130*, 3276–3277. (b) Campeau, L.-C.; Stuart, D. R.; Leclerc, J.-P.; Bertrand-Laperle, M.; Villemure, E.; Sun, H.-Y.; Lasserre, S.; Guimond, N.; Lecavallier, M.; Fagnou, K., Palladium-Catalyzed Direct Arylation of Azine and Azole *N*-Oxides: Reaction Development, Scope and Applications in Synthesis. *J. Am. Chem. Soc*. **2009**, *131* 3291–3306. (c) Li, C.; Li, P.; Yanga, J.; Wang, L., Palladium-catalyzed deamidative arylation of azoles with arylamides through a tandem decarbonylation–C–H functionalization. *Chem. Commun*., **2012**, *48*, 4214-4216. (d) Zhu, F.; Wang, Z.-X., Palladium-Catalyzed Coupling of Azoles or Thiazoles with Aryl Thioethers via C–H/C–S Activation. *Org. Lett*. **2015**, *17*, 1601–1604. (e) Yamada, S.; Murakami, K.; Itami, K., Regiodivergent Cross-Dehydrogenative Coupling of Pyridines and Benzoxazoles: Discovery of Organic Halides as Regio-Switching Oxidants. *Org. Lett.* **2016,** *18* (10), 2415-2418 (f) Piou, T.; Slutskyy, Y.; Kevin, N. J.; Sun, Z.; Xiao, D.; Kong, J., Direct Arylation of Azoles Enabled by Pd/Cu Dual Catalysis. *Org. Lett.* **2021**, *23*, 1996–2001.

(9) Selected examples of metal-free azole C–H functionalizations, see: He, T.; Li, H.; Li, P.; Wang, L., Direct amidation of azoles with formamides via metal-free C–H activation in the presence of *tert*-butyl perbenzoate. *Chem. Commun*., **2011**, *47*, 8946-8948; (b) Ahmed, J.; Sreejyothi, P.; Vijaykumar, G.; Jose, A.; Raj, M.; Mandal, S. K., A new face of phenalenyl-based radicals in the transition metal-free C–H arylation of heteroarenes at room temperature: trapping the radical initiator via C–C s-bond formation. *Chem. Sci.*, **2017**, *8*, 7798-7806; (c) Li, Z.-l.; Jin, L.-K.; Cai, C., Efficient synthesis of 2-substituted azoles: radical C–H alkylation of azoles with dicumyl peroxide, methylarenes and cycloalkanes under metal-free condition. *Org. Chem. Front*., **2017**, *4*, 2039-2043; (d) Qiu, Y.; Struwe, J.; Meyer, T. H.; Oliveira, J. C. A.; Ackermann, L., Catalyst- and Reagent-Free Electrochemical Azole C−H Amination. *Chem.–Eur. J*., **2018**, *24*, 12784-12789; (e) He, T.; Yu, L.; Zhang, L.; Wang, L.; Wang, M., Direct C2-Alkylation of Azoles with Alcohols and Ethers through Dehydrogenative Cross-Coupling under Metal-Free Conditions. *Org. Lett*., **2011**, *13*, 5016-5019; (f) Xu, W.-X.; Dai, X.-Q.; Weng, J.-Q., $K_2S_2O_8$-Mediated Hydroxyalkylation of Benzothiazoles with Alcohols in Aqueous Solution. *ACS Omega* **2019**, *4*, 11285-11292; (h) Lipp, A.; Lahm, G.; Opatz, T., Light Induced C–C Coupling of 2-Chlorobenzazoles with Carbamates, Alcohols, and Ethers. *J. Org. Chem*., **2016**, *81*, 4890.

(10) Selected examples of metal-catalyzed azole C–H Carboxylations, see: (a) Zhang, L.; Cheng, J.; Ohishi, T.; Hou, Z., Copper-Catalyzed Direct Carboxylation of C-H Bonds with Carbon Dioxide. *Angew. Chem. Int. Ed.* **2010**, *49*, 8670-8673. (b) Boogaerts, I. I. F.; Nolan, S. P., Carboxylation of C–H Bonds Using *N*-Heterocyclic Carbene Gold(I) Complexes. *J. Am. Chem. Soc.* **2010**, *132*, 8858–8859. (c) Boogaerts, I. I. F.; Fortman, G. C.; Furst, M. R. L.; Cazin, C. S. J.; Nolan, S. P., Carboxylation of N–H/C–H Bonds Using N-Heterocyclic Carbene Copper(I) Complexes. *Angew. Chem. Int. Ed.* **2010**, *49*, 8674-8677. (d) Inomata, H.; Ogata, K.; Fukuzawa, S.; Hou, Z., Direct C–H Carboxylation with Carbon Dioxide Using 1,2,3-Triazol-5-ylidene Copper(I) Complexes. *Org. Lett.* **2012**, *14*, 3986-3989. (e) Wang, W.; Zhang, G.; Lang, R.; Xia, C.; Li, F., pH-Responsive *N*-Heterocyclic Carbene Copper(I) Complexes: Syntheses and Recoverable Applications in the Carboxylation of Arylboronic Esters and Benzoxazole with Carbon Dioxide. *Green Chem.*, **2013**, *15*, 635-640. (f) Park, D.-A.; Ryu, J. Y.; Lee, J.; Hong, S., Bifunctional *N*-Heterocyclic Carbene Ligands for Cu-Catalyzed Direct C–H Carboxylation with CO_2. *RSC Adv*., **2017**, *7*, 52496–52502. (g) Chen, J.-H.; Deng, C.-H.; Fang, S.; Ma, J.-G.; Cheng, P., Binuclear Molybdenum Alkoxide as the Versatile Catalyst for the Conversion of Carbon Dioxide. *Green Chem.*, **2018**, *20*, 989-996.

(11) Selected examples of metal-free azole C–H Carboxylations, see: (a) Komoriya, S.; Kobayashi, S.; Osanai, K.; Yoshino, T.; Nagata, T.; Haginoya, N.; Nakamoto, Y.; Mochizuki, A.; Nagahara, T.; Suzuki, M.; Shimada, T.; Watanabe, K.; Isobe, Y.; Furugoori, T., Design, synthesis, and biological activity of novel factor Xa inhibitors: Improving metabolic stability by S1 and S4 ligand modification. *Bioorg. Med. Chem.* **2006**, *14*, 1309–1330. (b) Vechorkin, O.; Hirt, N.; Hu, X., Carbon Dioxide as the C1 Source for Direct C–H Functionalization of Aromatic Heterocycles. *Org. Lett.* **2010**, *12*, 3567-3569. (c) Fenner, S.; Ackermann, L., C–H carboxylation of heteroarenes with ambient CO_2. *Green Chem.*, **2016**, *18*, 3804–3807.

(12) https://scifinder-n.cas.org/; see Supporting Information for details.

(13) (a) Boger, D. L.; Fink, B. E.; Hedrick, M. P., Total Synthesis of Distamycin A and 2640 Analogues: A Solution-Phase Combinatorial Approach to the Discovery of New, Bioactive DNA Binding Agents and Development of a Rapid, High-Throughput Screen for

Determining Relative DNA Binding Affinity or DNA Binding Sequence Selectivity. *J. Am. Chem. Soc.* **2000**, *122*, 6382-6394.

(14) Emmert, M. H.; He, C. Q.; Shah, A. A.; Felten, S., Lewis acid mediated, mild C–H aminoalkylation of azoles via three component coupling. *Chem. Sci.*, **2021**, *12*, 3890-3897.

(15) (a) Dunetz, J. R.; Magano, J.; Weisenburger, G. A., Large-Scale Applications of Amide Coupling Reagents for the Synthesis of Pharmaceuticals. O*rg. Process Res. Dev.* 2**016,** *20*, 140−177. (b) Magano, J., Large-Scale Amidations in Process Chemistry: Practical Considerations for Reagent Selection and Reaction Execution. O*rg. Process Res. Dev. 2***022,***26,1*562−1689. (c) Brown, D. G.; Bostrom, J., Analysis of past and present synthetic methodologies on medicinal chemistry: where have all the new reactions gone? Miniperspective. J. *Med. Chem.* 2**016,** 59, 4443−4458. (d) Top 200 Drugs 2019- The Poster. Top 200 Drugs 2019 - The Poster - Pharma Excipients (accessed 2022-07-27). (e) Dhameliya, T. M.; Tiwari, R.; Banerjee, A.; Pancholia, S.; Sriram, D.; Panda, D.; Chakraborti, A. K., Benzo[d]thiazole-2-carbanilides as new anti-TB chemotypes: Design, synthesis, biological evaluation, and structure-activity relationship. *Eur. J.-Med. Chem.* **2018**, *155*, 364-380. (f) Pancholia, S.; Dhameliya, T. M.; Shah, P.; Jadhava, P. S.; Padma Sridevi, J.; Yogeshwari, P.; Sriram, D.; Chakraborti, A. K., Benzo[d]thiazol-2-yl(piperazin-1-yl)methanones as new antimycobacterial chemotypes: Design, synthesis, biological evaluation and 3D-QSAR studies. *Eur. J.-Med. Chem.* **2016**, *116*, 187-199. (g) Carey, J. S.; Laffan, D.; Thomson, C.; Williams, M. T., Analysis of the reactions used for the preparation of drug candidate molecules. *Org. Biomol. Chem.*, **2006**, *4*, 2337–2347. (h) Wang, Y.; Haight, I.; Gupta, R.; Vasudevan, A., What is in Our Kit? An Analysis of Building Blocks Used in Medicinal Chemistry Parallel Libraries. *J. Med. Chem.* **2021**, *64*, 17115–17122.

(16) MacMillan, D. S.; Murray, J.; Sneddon, H. F.; Jamieson, C.; Watson, A. J. B., Evaluation of alternative solvents in common amide coupling reactions: replacement of dichloromethane and *N*,*N*-dimethylformamide. *Green Chem.*, **2013**, *15*, 596-600.

(17) RDKit: Open-source cheminformatics. https://www.rdkit.org. https://doi.org/10.5281/zenodo.591637.

(18) van der Maaten, L.; Hinton, G., Visualizing Data Using T-SNE. *J. Mach. Learn. Res.* **2008**, *9* (Nov), 2579– 2605.

(19) Similar workflows are reported in literature, see: Kariofillis, S. K.; Jiang, S.; Żurański, A. M.; Gandhi, S. S.; Martinez Alvarado, J. I.; Doyle, A. G., Using Data Science To Guide Aryl Bromide Substrate Scope Analysis in a Ni/Photoredox-Catalyzed Cross-Coupling with Acetals as Alcohol-Derived Radical Sources. *J. Am. Chem. Soc.* **2022**, *144*, 1045–1055.

(20) (a) Balasubramaniam, S.; Aidhen, I. S., The Growing Synthetic Utility of the Weinreb Amide. *Synthesis* **2008**, *23*, 3707-3738. (b) Kalepu, J.; Pilarski, L. T., Weinreb Amides as Directing Groups for Transition Metal-Catalyzed C-H Functionalizations. *Molecules* **2019**, *24* (5), 830-852. (c) Senatore, R.; Ielo, L.; Monticelli, S.; Castoldi, L.; Pace, V., Weinreb Amides as Privileged Acylating Agents for Accessing α-Substituted Ketones. *Synthesis* **2019**, *51* (14), 2792-2808. (d) Nowak, M., Weinreb Amides. *Synlett* **2015**, *26*, 561–562. (e) Aitken, R. A.; Inwood, R. A., 4.04 - Oxazoles. In: Comprehensive Heterocyclic Chemistry IV, Editors: Black, D.; Cossy, J.; Stevens, C. V., *Elsevier* **2022**, *4*, 435-481. https://doi.org/10.1016/B978-0-12-818655-8.00157-8. (f) Varvounis, G.; Gkalpinos, V.; Theodorakopoulou, P.; Tsemperlidou, E., 4.02 – Imidazoles. In: Comprehensive Heterocyclic Chemistry IV, Editors: Black, D.; Cossy, J.; Stevens, C. V., *Elsevier* **2022**, *4*, 113-307. https://doi.org/10.1016/B978-0-12-818655-8.00140-2.

(21) (a) Isin, E. M.; Elmore, C. S.; Nilsson, G. N.; Thompson, R. A.; Weidolf, L., Use of Radiolabeled Compounds in Drug Metabolism and Pharmacokinetic Studies. *Chem. Res. Toxicol.* **2012**, *25*, 532−542. (b) Elmore, C. S.; Bragg, R. A., Isotope Chemistry; a Useful Tool in the Drug Discovery Arsenal. *Bioorg. Med. Chem. Lett.* **2015**, *25*, 167−171. (c) Marathe, P. H.; Shyu, W. C.; Humphreys, W. G., The Use of Radiolabeled Compounds for ADME Studies in Discovery and Exploratory Development. *Curr. Pharm. Des.* **2004**, *10*, 2991−3008. (d) Elmore, C. S., The Use of Isotopically Labeled Compounds in Drug Discovery. *Annu. Rep. Med. Chem*. **2009**, *44*, 515−534. (e) Ruiz-Garcia, A.; Bermejo, M.; Moss, A.; Casabo, V. G., Pharmacokinetics in Drug Discovery. *J. Pharm. Sci.* **2008**, *97*, 654−690. (f) Zhang, Z.; Tang, W., Drug Metabolism in Drug Discovery and Development. *Acta Pharm. Sin. B* **2018**, *8*, 721−732. (g) (4) (a) Tu, Z.; Mach, R. H., C-11 Radiochemistry in Cancer Imaging Applications. *Curr. Top. Med. Chem.* **2010**, *10*, 1060−1095. (h) Ahamed, M.; Verbeek, J.; Funke, U.; Lecina, J.; Verbruggen, A.; Bormans, G., Recent Progress in Metal Catalyzed Direct Carboxylation of Aryl Halides and Pseudo Halides Employing CO_2: Opportunities for ^{11}C Radiochemistry. *ChemCatChem* **2016**, *8*, 3692−3700.

(22) (a) Destro, G.; Loreau, O.; Marcon, E.; Taran, F.; Cantat, T.; Audisio, D., Dynamic Carbon Isotope Exchange of Pharmaceuticals with Labeled CO_2. *J. Am. Chem. Soc.* **2019**, *141*, 780−784. (b) Bragg, R. A.; Sardana, M.; Artelsmair, M.; Elmore, C. S., New Trends and Applications in Carboxylation for Isotope Chemistry. *J. Labelled Compd. Radiopharm.* **2018**, *61*, 934−948. (c) Tortajada, A.; Duan, Y.; Sahoo, B.; Cong, F.; Toupalas, G.; Sallustrau, A.; Loreau, O.; Audisio, D.; Martin, R., Catalytic Decarboxylation/Carboxylation Platform for Accessing Isotopically Labeled Carboxylic Acids. *ACS Catal.* **2019**, *9*, 5897−5901.

(23) (a) Papadopoulos, E. P.; Schupbachechorkin, C. M., Reactions of azoles with isocyanates at elevated temperature. *J. Org. Chem.* **1979**, *44*, 99-104. (b) Fukumoto, Y.; Shiratani, M.; Noguchi, H.; Chatani, N., Iridium-Catalyzed Direct Amidation of Imidazoles at the C-2 Position with Isocyanates in the Presence of Hydrosilanes Leading to Imidazole-2-Carboxamides. *Synthesis* **2021**, *53*, 3011–3018.

(24) Li, Z.; Mayer, R. J.; Ofial, A.R.; Mayr, H., From Carbodiimides to Carbon Dioxide: Quantification of the Electrophilic Reactivities of Heteroallenes. *J. Am. Chem. Soc.* **2020**, *142*, 8383–8402.